# VECSEL gain characterization

**Mario Mangold,[1,*] Valentin J. Wittwer,[1] Oliver D. Sieber,[1] Martin Hoffmann,[1] Igor L. Krestnikov,[2] Daniil A. Livshits,[2] Matthias Golling,[1] Thomas Südmeyer,[1] and Ursula Keller[1]**

[1]*Department of Physics, Institute for Quantum Electronics, ETH Zurich, 8093 Zurich, Switzerland*
[2]*Innolume GmbH, Konrad-Adenauer-Allee 11, 44263 Dortmund, Germany*
[*]*mangoldm@phys.ethz.ch*

**Abstract:** We present the first full gain characterization of two vertical external cavity surface emitting laser (VECSEL) gain chips with similar designs operating in the 960-nm wavelength regime. We optically pump the structures with continuous-wave (cw) 808-nm radiation and measure the nonlinear reflectivity for 130-fs and 1.4-ps probe pulses as function of probe pulse fluence, pump power, and heat sink temperature. With this technique we are able to measure the saturation behavior for VECSEL gain chips for the first time. The characterization with 1.4-ps pulses resulted in saturation fluences of 40-80 μJ/cm$^2$, while probing with 130-fs pulses yields reduced saturation fluences of 30-50 μJ/cm$^2$ for both structures. For both pulse durations this is lower than previously assumed. A small-signal gain of up to 5% is obtained with this technique. Furthermore, in a second measurement setup, we characterize the spectral dependence of the gain using a tunable cw probe beam. We measure a gain bandwidth of over 26 nm for both structures, full width at half maximum.

©2012 Optical Society of America

**OCIS codes:** (140.7260) Vertical cavity surface emitting lasers; (140.4050) Mode-locked lasers.

## References and links

1. U. Keller, K. J. Weingarten, F. X. Kärtner, D. Kopf, B. Braun, I. D. Jung, R. Fluck, C. Hönninger, N. Matuschek, and J. Aus der Au, “Semiconductor saturable absorber mirrors (SESAMs) for femtosecond to nanosecond pulse generation in solid-state lasers,” IEEE J. Sel. Top. Quantum Electron. **2**(3), 435–453 (1996).
2. S. Hoogland, S. Dhanjal, A. C. Tropper, J. S. Roberts, R. Haring, R. Paschotta, F. Morier-Genoud, and U. Keller, “Passively mode-locked diode-pumped surface-emitting semiconductor laser,” IEEE Photon. Technol. Lett. **12**(9), 1135–1137 (2000).
3. U. Keller and A. C. Tropper, “Passively modelocked surface-emitting semiconductor lasers,” Phys. Rep. **429**(2), 67–120 (2006).
4. A. H. Quarterman, K. G. Wilcox, V. Apostolopoulos, Z. Mihoubi, S. P. Elsmere, I. Farrer, D. A. Ritchie, and A. Tropper, “A passively mode-locked external-cavity semiconductor laser emitting 60-fs pulses,” Nat. Photonics **3**(12), 729–731 (2009).
5. P. Klopp, U. Griebner, M. Zorn, and M. Weyers, “Pulse repetition rate up to 92 GHz or pulse duration shorter than 110 fs from a mode-locked semiconductor disk laser,” Appl. Phys. Lett. **98**(7), 071103 (2011).
6. D. Lorenser, D. J. H. C. Maas, H. J. Unold, A.-R. Bellancourt, B. Rudin, E. Gini, D. Ebling, and U. Keller, “50-GHz passively mode-locked surface-emitting semiconductor laser with 100 mW average output power,” IEEE J. Quantum Electron. **42**(8), 838–847 (2006).
7. B. Rudin, V. J. Wittwer, D. J. H. C. Maas, M. Hoffmann, O. D. Sieber, Y. Barbarin, M. Golling, T. Südmeyer, and U. Keller, “High-power MIXSEL: an integrated ultrafast semiconductor laser with 6.4 W average power,” Opt. Express **18**(26), 27582–27588 (2010).
8. D. J. H. C. Maas, A.-R. Bellancourt, B. Rudin, M. Golling, H. J. Unold, T. Südmeyer, and U. Keller, “Vertical integration of ultrafast semiconductor lasers,” Appl. Phys. B **88**(4), 493–497 (2007).
9. P. Klopp, F. Saas, M. Zorn, M. Weyers, and U. Griebner, “290-fs pulses from a semiconductor disk laser,” Opt. Express **16**(8), 5770–5775 (2008).
10. K. G. Wilcox, M. Butkus, I. Farrer, D. A. Ritchie, A. Tropper, and E. U. Rafailov, “Subpicosecond quantum dot saturable absorber mode-locked semiconductor disk laser,” Appl. Phys. Lett. **94**(25), 251105 (2009).

#159130 - $15.00 USD Received 2 Dec 2011; revised 19 Jan 2012; accepted 20 Jan 2012; published 3 Feb 2012

11. K. G. Wilcox, A. H. Quarterman, H. Beere, D. A. Ritchie, and A. C. Tropper, "High peak power femtosecond pulse passively mode-locked vertical-external-cavity surface-emitting laser," IEEE Photon. Technol. Lett. **22**(14), 1021–1023 (2010).
12. M. Hoffmann, O. D. Sieber, V. J. Wittwer, I. L. Krestnikov, D. A. Livshits, Y. Barbarin, T. Südmeyer, and U. Keller, "Femtosecond high-power quantum dot vertical external cavity surface emitting laser," Opt. Express **19**(9), 8108–8116 (2011).
13. S. Pekarek, T. Südmeyer, S. Lecomte, S. Kundermann, J. M. Dudley, and U. Keller, "Self-referenceable frequency comb from a gigahertz diode-pumped solid-state laser," Opt. Express **19**(17), 16491–16497 (2011).
14. M. C. Stumpf, S. Pekarek, A. E. H. Oehler, T. Südmeyer, J. M. Dudley, and U. Keller, "Self-referencable frequency comb from a 170-fs, 1.5-μm solid-state laser oscillator," Appl. Phys. B **99**(3), 401–408 (2010).
15. R. Aviles-Espinosa, G. Filippidis, C. Hamilton, G. Malcolm, K. J. Weingarten, T. Südmeyer, Y. Barbarin, U. Keller, S. I. C. O. Santos, D. Artigas, and P. Loza-Alvarez, "Compact ultrafast semiconductor disk laser: targeting GFP based nonlinear applications in living organisms," Biomed. Opt. Express **2**(4), 739–747 (2011).
16. M. Hoffmann, O. D. Sieber, D. J. H. C. Maas, V. J. Wittwer, M. Golling, T. Südmeyer, and U. Keller, "Experimental verification of soliton-like pulse-shaping mechanisms in passively mode-locked VECSELs," Opt. Express **18**(10), 10143–10153 (2010).
17. R. Paschotta, R. Häring, A. Garnache, S. Hoogland, A. C. Tropper, and U. Keller, "Soliton-like pulse-shaping mechanism in passively mode-locked surface-emitting semiconductor lasers," Appl. Phys. B **75**(4-5), 445–451 (2002).
18. F. X. Kärtner, I. D. Jung, and U. Keller, "Soliton Mode-Locking with Saturable Absorbers," IEEE J. Sel. Top. Quantum Electron. **2**(3), 540–556 (1996).
19. D. J. H. C. Maas, B. Rudin, A.-R. Bellancourt, D. Iwaniuk, S. V. Marchese, T. Südmeyer, and U. Keller, "High precision optical characterization of semiconductor saturable absorber mirrors," Opt. Express **16**(10), 7571–7579 (2008).
20. O. D. Sieber, V. J. Wittwer, M. Mangold, M. Hoffmann, M. Golling, T. Südmeyer, and U. Keller, "Femtosecond VECSEL with tunable multi-gigahertz repetition rate," Opt. Express **19**(23), 23538–23543 (2011).
21. K. L. Hall, E. R. Thoen, and E. P. Ippen, "Nonlinearities in Active Media," in *Semiconductors and Semimetals*, G. Elsa, and K. Alan, eds. (Elsevier, 1998), pp. 83–160.
22. D. Maas, "MIXSELs - A New Class of Ultrafast Semiconductor Lasers," dissertation (ETH Zurich, Nr. 18121, Hartung-Gorre Verlag, Konstanz, 2009).
23. G. J. Spühler, K. J. Weingarten, R. Grange, L. Krainer, M. Haiml, V. Liverini, M. Golling, S. Schon, and U. Keller, "Semiconductor saturable absorber mirror structures with low saturation fluence," Appl. Phys. B **81**(1), 27–32 (2005).
24. Z. G. Wang, F. Q. Liu, J. B. Liang, and B. Xu, "Self-assembled InAs/GaAs quantum dots and quantum dot laser," Sci. China A **43**(8), 861–870 (2000).
25. R. Häring, R. Paschotta, A. Aschwanden, E. Gini, F. Morier-Genoud, and U. Keller, "High–power passively mode–locked semiconductor lasers," IEEE J. Quantum Electron. **38**(9), 1268–1275 (2002).
26. M. Haiml, R. Grange, and U. Keller, "Optical characterization of semiconductor saturable absorbers," Appl. Phys. B **79**(3), 331–339 (2004).
27. D. J. H. C. Maas, A. R. Bellancourt, M. Hoffmann, B. Rudin, Y. Barbarin, M. Golling, T. Südmeyer, and U. Keller, "Growth parameter optimization for fast quantum dot SESAMs," Opt. Express **16**(23), 18646–18656 (2008).
28. O. E. Martinez, R. L. Fork, and J. P. Gordon, "Theory of passively modelocked lasers for the case of a nonlinear complex propagation coefficient," J. Opt. Soc. Am. B **2**(5), 753–760 (1985).
29. L. M. Frantz and J. S. Nodvik, "Theory of pulse propagation in a laser amplifier," J. Appl. Phys. **34**(8), 2346–2349 (1963).
30. E. R. Thoen, E. M. Koontz, M. Joschko, P. Langlois, T. R. Schibli, F. X. Kärtner, E. P. Ippen, and L. A. Kolodziejski, "Two-photon absorption in semiconductor saturable absorber mirrors," Appl. Phys. Lett. **74**(26), 3927–3929 (1999).
31. M. Haiml, U. Siegner, F. Morier-Genoud, U. Keller, M. Luysberg, R. C. Lutz, P. Specht, and E. R. Weber, "Optical nonlinearity in low-temperature-grown GaAs: Microscopic limitations and optimization strategies," Appl. Phys. Lett. **74**(21), 3134–3136 (1999).
32. M. E. Barnes, Z. Mihoubi, K. G. Wilcox, A. H. Quarterman, I. Farrer, D. A. Ritchie, A. Garnache, S. Hoogland, V. Apostolopoulos, and A. C. Tropper, "Gain bandwidth characterization of surface-emitting quantum well laser gain structures for femtosecond operation," Opt. Express **18**(20), 21330–21341 (2010).
33. C. Borgentun, J. Bengtsson, and A. Larsson, "Direct measurement of the spectral reflectance of OP-SDL gain elements under optical pumping," Opt. Express **19**(18), 16890–16897 (2011).
34. A. H. Quarterman, K. G. Wilcox, V. Apostolopoulos, Z. Mihoubi, M. Barnes, I. Farrer, D. A. Richie, and A. Tropper, "Gain Saturation in 60-fs Mode-Locked Semiconductor Laser" (Optical Society of America, 2010), p. CMY4.
35. G. P. Agrawal, "Effect of gain dispersion on ultrashort pulse amplification in semiconductor laser amplifiers," IEEE J. Quantum Electron. **27**(6), 1843–1849 (1991).
36. S. Hoogland, V. Sukhovatkin, I. Howard, S. Cauchi, L. Levina, and E. H. Sargent, "A solution-processed 1.53 µm quantum dot laser with temperature-invariant emission wavelength," Opt. Express **14**(8), 3273–3281 (2006).



#159130 - $15.00 USD Received 2 Dec 2011; revised 19 Jan 2012; accepted 20 Jan 2012; published 3 Feb 2012


(C) 2012 OSA

37. N. N. Ledentsov, N. Kirstaedter, M. Grundmann, D. Bimberg, V. M. Ustinov, I. V. Kochnev, P. S. Kop'ev, and Z. I. Alferov, “Three-dimensional arrays of self-ordered quantum dots for laser applications,” Microelectron. J. **28**(8-10), 915–931 (1997).
38. J. Hader, J. V. Moloney, S. W. Koch, and W. W. Chow, “Microscopic modeling of gain and luminescence in semiconductors,” IEEE J. Sel. Top. Quantum Electron. **9**(3), 688–697 (2003).

## 1. Introduction

After the first demonstration of semiconductor saturable absorber mirror (SESAM) [1] modelocked vertical external cavity surface emitting lasers (VECSEL) in 2000 [2], the performance in terms of output power, repetition rate and pulse duration substantially improved during the following six years [3]. To date the shortest pulse duration generated by a VECSEL has been 60 fs at less than 35 mW average output power operating in multi-pulsing [4] and 107 fs at 3 mW in fundamental modelocking [5]. A pulse repetition rate as high as 50 GHz was achieved at 100 mW average output power in 3.3-ps-pulses [6]. Recently, up to 6.4 W of average power with a 28-ps pulse duration was demonstrated with a MIXSEL (modelocked integrated external-cavity surface emitting laser), for which the SESAM is integrated into the VECSEL structure [7, 8]. Average power scaling in the femtosecond regime resulted in up to 150 mW in the sub-500-fs regime [9–12] and even more than 1 W with 784-fs pulses [12].

Ideally sub-500-fs pulses are required for compact frequency combs [13, 14] and biomedical imaging applications [15]. A quantitative understanding of the pulse formation process is essential for further power scaling and numerical simulations have been successfully used for a better understanding [16]. SESAM modelocked VECSELs experience strong dynamic gain and absorber saturation, which leads to a total nonlinear phase change that can be compensated with positive group delay dispersion (GDD) [17] in analogy to soliton modelocking [18]. This pulse formation process was confirmed experimentally in the picosecond regime [16]. Key parameters for the pulse formation, such as saturation fluence and modulation depth of the SESAM, can be characterized precisely [19], but gain saturation parameters of optically-pumped VECSEL structures have not been measured so far.

Here we present the first full gain characterization of VECSEL gain structures that resulted in high-power femtosecond pulses [12] and broadly tunable femtosecond pulses at gigahertz pulse repetition rates [20]. Using two high-precision reflectivity measurement techniques we were able to characterize the saturation behavior and the small-signal gain and the spectral gain bandwidth. In contrast to previously assumed values of 160 μJ/cm$^2$ [17] for the saturation fluence, we measured saturation fluences of 30-80 μJ/cm$^2$ for our structures. Those are strongly dependent on the probe pulse duration [21], pump intensities and the temperature of the structure. Small-signal gain over 5% was measured with two different techniques and both structures exhibit a gain bandwidth of more than 26 nm, full width at half maximum (FWHM).

## 2. VECSEL gain structures

For the characterization of the gain properties two different samples were used. The basic design of the gain chip is shown in Fig. 1.

A distributed Bragg reflector (DBR) for the pump wavelength (808 nm) reflects the unabsorbed pump light, reducing heat deposition in the structure and increasing efficiency. The DBR for the laser wavelength acts as a flat cavity mirror.

#159130 - $15.00 USD Received 2 Dec 2011; revised 19 Jan 2012; accepted 20 Jan 2012; published 3 Feb 2012
(C) 2012 OSA

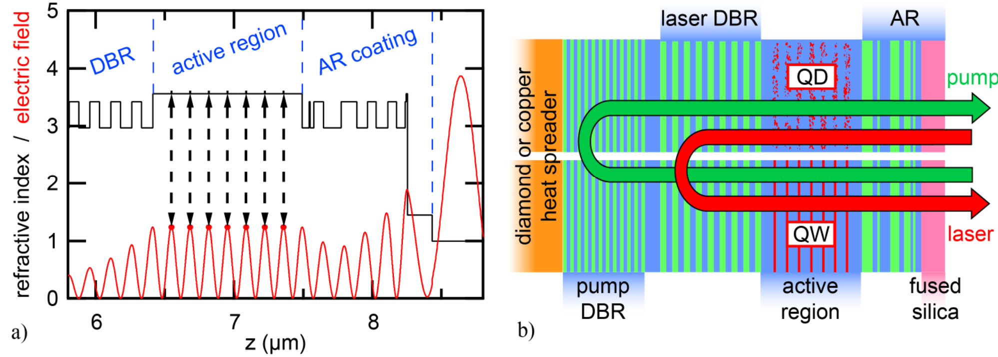


Fig. 1. VECSEL gain chip structure: a) Top part of epitaxial layer structure with the corresponding refractive index profile (black). The active region either consists of quantum dots (QDs) or quantum wells (QWs), which are placed in the antinodes of the standing wave pattern of the electric field (red) b) Full VECSEL structure with heat-spreader and DBRs for the pump and emission wavelength. On top of the active region a combined semiconductor/dielectric anti-reflection (AR) section is placed to achieve flat group-delay dispersion around the emission wavelength.

The active region is grown on top of the laser DBR centered around 960 nm and QD- and QW-based structures are presented. Figure 1a presents the refractive indices of the QD-structure and the corresponding standing wave pattern of the electric field. The QWs or QD layers are placed in the antinodes. The field enhancement $\Gamma$ describes the normalized field strength averaged for the gain layers in the structure [22, 23]. In resonant structures without a top-coating $\Gamma = 4$, while $\Gamma \approx 0.3$ holds for anti-resonant structures in GaAs. On top of the active region an anti-reflection (AR) section is grown and a fused silica (FS) layer is deposited by PECVD (plasma-enhanced chemical vapor deposition) (see Fig. 1b), which results in a field enhancement of $\Gamma \approx 1.2$ and a flat GDD over 30-nm bandwidth centered at the lasing wavelength.

**Table 1. Comparison of the Properties of the Characterized VECSEL Structures**

| VECSEL gain chip | structure 1 | structure 2 |
|---|---|---|
| **growth** | MBE-grown<br>Innolume GmbH, Germany | MBE-grown<br>FIRST cleanroom facility, ETH Zurich |
| **laser DBR** | 30-pair DBR AlAs/$Al_{0.2}Ga_{0.8}As$ (adapted to 960 nm (QD) / 950 nm (QW)) | |
| **pump DBR** | 15-pair DBR AlAs/$Al_{0.2}Ga_{0.8}As$ (adapted to 808 nm) | |
| **active region** | 7 groups of 9 indium arsenide (InAs)<br>QD layers in GaAs<br>Stranski-Krastanov growth [24] | 7 indium gallium arsenide ($In_{0.17}GaAs$)<br>QW layers (4.5 nm) in GaAs |
| **field enhancement** | 1.25 | 1.14 |
| **AR coating** | 14-layer AR section:<br>12 AlAs/$Al_{0.2}Ga_{0.8}As$ layers; GaAs cap layer; PECVD-deposited fused silica layer | |
| **modelocking results** | $P_{av}$ = 1.05 W, $\tau_p$ = 784 fs,<br>$f_{rep}$ = 5.4 GHz [12] | $P_{av}$ = 169 mW, $\tau_p$ = 625 fs,<br>$f_{rep}$ = 6.5 – 11.3 GHz (tunable) [20] |

This supports the generation of ultrashort pulses [12]. For better heat-removal both structures were grown in reverse order and were soldered to a CVD-diamond or copper heat-spreader. The substrate is removed with chemical wet-etching [25], before the FS layer is deposited. Table 1 presents structure and growth parameters of the two VECSELs under investigation. We refer to recent publications [12] and [20] for the more detailed description of both structures and the modelocked performance.

#159130 - $15.00 USD Received 2 Dec 2011; revised 19 Jan 2012; accepted 20 Jan 2012; published 3 Feb 2012
(C) 2012 OSA

## 3. Theory of gain saturation measurements

The following model for gain saturation in VECSEL structures is based on the one describing absorber saturation in SESAMs [26, 27]. This has been extremely successful to determine macroscopic parameters from the measurements of saturable absorbers in a broad range of probe pulse durations even though a very simple two-level approximation was used. These macroscopic parameters then can be used for pulse propagation simulations. For analytical calculations of gain saturation the band structure of the semiconductor gain medium can be approximated by a two-level system, where we neglect effects such as intra-band relaxations, trapping and recombination and also temperature-dependent effects and carrier diffusion in the gain structure. A traveling wave model is applied to a two-level system relying on rate equations. This holds for a long recovery time of the population inversion compared to the length of the pulse inducing the emission. With these assumptions a simple partial differential equation can be found for the dynamics of the gain with $g \ll 1$ [17, 28]:

$$\frac{\partial g}{\partial t} = -\frac{g - g_{ss}}{\tau_g} - \frac{g \cdot I}{F_{sat}}. \tag{1.1}$$

The saturation fluence $F_{sat}$ is a macroscopic and material-dependent parameter. The parameter $g$ is the gain coefficient, which is in the order of a few percent, $g_{ss}$ is the small-signal gain, which represents the gain coefficient without saturation effects, $\tau_g$ is the upper state lifetime of the gain and $I$ the intensity of the amplified beam. Note that the power amplification factor is defined as $G = \exp(g)$ and all following gain coefficients are defined for power. The upper-state lifetime in semiconductor lasers is typically in the nanosecond regime, hence the amplified pulses are several orders of magnitude shorter and therefore spontaneous emission effects can be neglected within the interaction time with the pulse. Regarding very small fluences, the pulse energy $E_{p,in}$ is increased by the power amplification factor for unsaturated gain:

$$E_{p,out} = E_{p,in} \exp\left(g_{ss}\right). \tag{1.2}$$

For higher pulse energies the general case for gain saturation is well described by the Frantz-Nodvik-equation [29]:

$$\exp\left[g\left(F\right)\right] = \frac{F_{sat}}{F} \ln\left\{1 + \exp\left(g_{ss}\right)\left[\exp\left(\frac{F}{F_{sat}}\right) - 1\right]\right\}. \tag{1.3}$$

The parameter $F_{sat}$ is defined as the fluence, at which the gain has dropped to approximately (1-1/e) ≈ 63% of its initial value, assuming $g < 10\%$. The Frantz-Nodvick equation is valid for both saturable gain and absorption. For a better comparison, the saturation fluences in SESAM characterization and gain saturation are defined identically [26].

Another important parameter that has to be taken into account is induced absorption (IA). It occurs not only for SESAMs [26, 30], but also for the VECSEL gain chips. For short pulse durations, two-photon absorption (TPA) is its main contribution. For longer pulse durations, other contributions induced by thermal effects, free-carrier absorption, and charge accumulation can become significant [26]. IA causes a drop in reflectivity at high fluences and this has to be included in the model function. In case of SESAM measurements, the saturation of the absorption and IA have opposite signs, which enable a simple separation of both effects [19]. In contrast, for optically-pumped VECSELs, both effects decrease the reflectivity, and it is very challenging to separate one effect from the other.

Furthermore for a correct fit-function of the gain saturation behavior, an additional parameter has to be considered. The gain chip has a certain amount of losses (well below 0.5%) in the unpumped and highly saturated state because of residual losses of the Bragg

#159130 - $15.00 USD Received 2 Dec 2011; revised 19 Jan 2012; accepted 20 Jan 2012; published 3 Feb 2012
(C) 2012 OSA

mirror and scattering losses from rough interfaces [31]. The corresponding reflectivity is a small amount below 100% and is called $R_{ns}$ [3]. A reflectivity measurement without pumping, in which the gain chip shows SESAM-like reflectivity behavior, is used to determine the parameter $R_{ns}$.

Finally in analogy to the SESAM characterization presented by Haiml *et al.* [26] we need to take into account the Gaussian mode profile. The gain saturation model function relies on Eq. (1.3). The reflectivity model function $R^{\mathrm{FlatTop}}$ for a spatial flat-top intensity profile of the beam is

$$R^{\mathrm{FlatTop}}(F) = \exp\left[g(F)\right] = R_{ns}\frac{F_{sat}}{F}\ln\left\{1+\exp\left(\frac{R_{ss}}{R_{ns}}\right)\left[\exp\left(\frac{F}{F_{sat}}\right)-1\right]\right\}\exp\left(-\frac{F}{F_2}\right), \quad (1.4)$$

with the parameter $F_2$ as the fluence at which the reflectivity dropped to (1/e) ≈37% because of effects of IA. $R_{ss}$ represents the reflectivity of the small-signal gain. A flat-top beam exhibits a constant spatial fluence of radius $w$ defined as $F = E_p/w^2\pi$. However in most cases the laser beam exhibits a spatial Gaussian intensity distribution $F^{\mathrm{Gauss}}(r) = F_0 \exp(-2r^2/w^2)$. For the same pulse energy $E_p$, the peak fluence for a Gaussian beam is a factor of two higher than for the flat-top fluence and therefore saturation effects become significant at lower fluences. The adaption for a Gaussian intensity profile of the pulse is included in the fit by

$$R^{\mathrm{Gauss}}(F) = \int_0^1 \mathrm{d}z R^{\mathrm{FlatTop}}(2Fz), \quad (1.5)$$

with $z = 2F \exp(-2r^2/w^2)$ and $\mathrm{d}z = -8r/w^2 \exp(-2r^2/w^2)\mathrm{d}r$. For the full mathematical description please refer to [26].

Taking into account all the parameters, Fig. 2 depicts the final model function $R^{\mathrm{Gauss}}$ and an additional curve for the reflectivity behavior without the influence of IA. Reflectivities larger than 100% can be regarded as amplification.

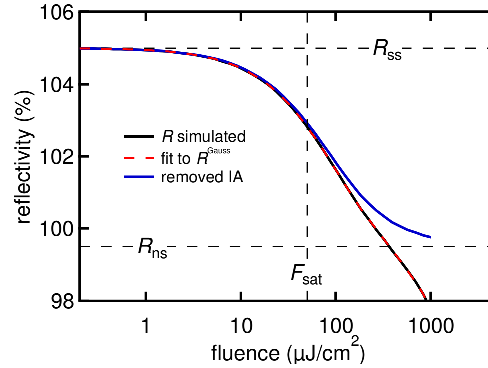


Fig. 2. Model for gain saturation: simulated reflectivity (black) is fitted to Eq. (1.5) (red dashed), accounting for a spatial Gaussian intensity distribution. From unpumped VECSEL measurements the parameter $R_{ns}$ can be extracted and inserted in Eq. (1.4). With this fit, the small-signal gain reflectivity $R_{ss,}$ the saturation fluence $F_{sat}$ and the strength of induced absorption $F_2$ are determined. Removing the influence of IA results in the pure gain saturation curve (blue).

## 4. Experimental techniques

### *4.1 Setup for gain saturation measurements*

A precise characterization of the saturation fluences of VECSEL gain chips requires a setup for measuring the reflectivity of a sample over a fluence range of typically four orders of

#159130 - $15.00 USD Received 2 Dec 2011; revised 19 Jan 2012; accepted 20 Jan 2012; published 3 Feb 2012
(C) 2012 OSA

magnitude. The setup is an adaption to the high-precision reflectivity SESAM characterization presented by Maas *et al.* [19].

Figure 3a presents the measurement setup. The pulsed laser source for the experiments is a modelocked Ti:sapphire laser (Spectra Physics Tsunami), configurable to emit 130-fs or 1.4-ps pulses at 960 nm. A Faraday isolator is used to avoid back reflections into the laser cavity, which can cause lasing instabilities. The combination of a controllable rotating and a fixed polarizing beamsplitter (PBS1) and (PBS2) allow for an adjustable change in fluence over four orders of magnitude while providing a transmission bandwidth of >100 nm. This is useful for spectral gain characterization, as described in Section 4.2.

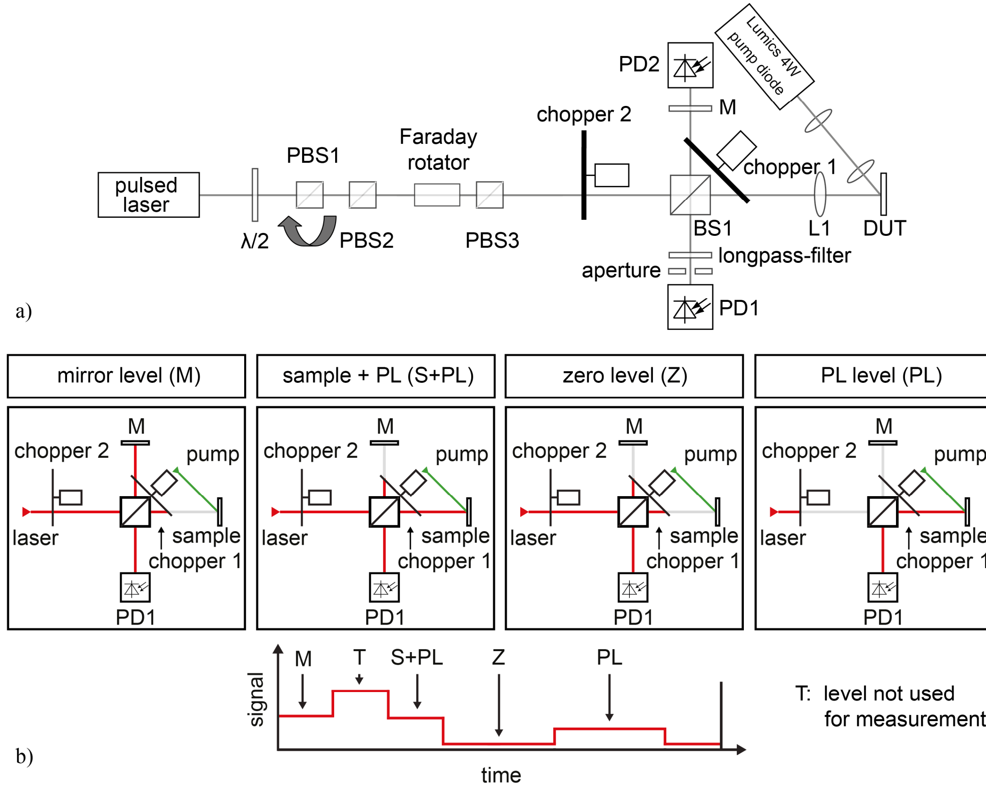


Fig. 3. Principle for gain saturation characterization: a) Measurement setup analogous to [19] with additional modifications for gain measurements: pump configuration with a 4 W pump diode at an angle of incidence of 45°; chopper 2 for adapted signal analysis, aperture and longpass-filter for suppression of the photoluminescence (PL) at PD1 b) Signal analysis scheme: Two phase-locked choppers ($f_{\text{chopper1}} = 2\, f_{\text{chopper2}}$) separate four distinguishable signals (top), which form the recorded signal (bottom). The PL of the gain chip is accounted for and the sample signal is finally compared to the signal of a high-reflective mirror of known reflectivity. 150 signal iterations yield the reflectivity of the gain chip.

After passing chopper 2, the beam is split in a non-polarizing beam-splitter (BS1) and the output of one port is guided on a high-reflective mirror (M). The output of the other port is focused onto the sample (L1: f = 20 mm) to achieve spot sizes below 20 µm in diameter and thus fluences of up to 1.1 mJ/cm$^2$ at the position of the device under test (DUT). The reflected beams from the DUT and the reference mirror M are overlapped in the third output port of the beam-splitter for detection with a standard fast photodiode (PD1) together with an adjustable trans-impedance amplifier and a digitizing card. A chopper wheel (chopper 1) is positioned such that the two ports of the beam-splitter are chopped synchronously. A

#159130 - $15.00 USD Received 2 Dec 2011; revised 19 Jan 2012; accepted 20 Jan 2012; published 3 Feb 2012
(C) 2012 OSA

sensitive photodiode (PD2) is placed behind the HR to record long-term (> 5s) laser power fluctuations and control the absolute fluences at the sample position [19].

The reflectivity of the gain chip can be extracted by calibration using a dielectric mirror of known reflectivity. However, in the small fluence regime photoluminescence (PL) from the pumped structure has to be accounted for, as its intensity on PD1 can become comparable to the signal itself. We therefore use a configuration with two phase-locked choppers, in which chopper 2 rotates at half the frequency of chopper 1, which enables measuring the PL intensity. To further reduce the PL, a longpass filter (cut-off at 900 nm) and an aperture are introduced in front of the detector. Four different signal levels (see Fig. 3b) arise from the different chopper configurations and enable both triggering of the iterative data analysis and extracting the reflectivity of the pumped gain chip with

$$R = \frac{(S + PL) - PL - Z}{M - Z}. \quad (1.6)$$

Averaging over 150 signal iterations yields the final measurement point.

The gain chip is pumped with a standard laser diode at 808 nm under 45°, resulting in an elliptical pump spot with a semi-minor axis of 60 µm. As the probe beam exhibits only 20 µm diameter, a nearly constant pump intensity over the spatial extention of the probe is obtained. With a maximum pump power of 3.42 W, this results in an average pump intensity of 74 kW/cm$^2$ at the probe laser spot.

### *4.2 Setup for spectral gain characterization*

A full characterization of a VECSEL gain structure requires a measurement of the spectral behavior of the gain. A sufficiently large amplification bandwidth is crucial for the generation of ultra-short pulses and optimized cavity outcoupling rates can be obtained from the amount of unsaturated gain.

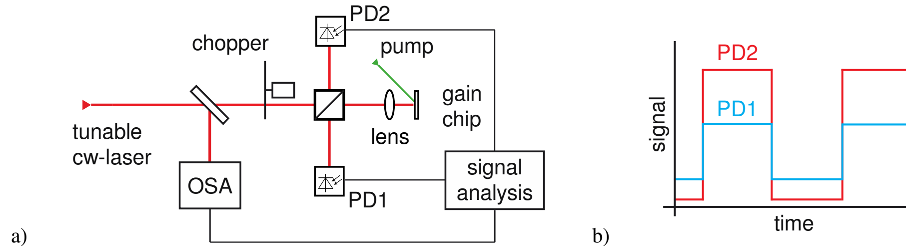


Fig. 4. Principle for spectral gain characterization: a) Measurement setup: The beam from a tunable cw Ti:Sapphire laser is split in a 50:50 beam-splitter. A reference signal is recorded directly on photodetector PD2. The beam of the other output arm is focused on the pumped gain chip and the amplified signal is recorded on detector PD1. b) Schematic signal from both detectors. A chopper is inserted to measure the signal-offset of PD1 to account for photoluminescence (PL).

In contrast to a spectro-temporal technique under operating conditions [32] we present a characterization method that relies on a wavelength dependent reflectivity measurement of a pumped gain chip (Fig. 4a), presented in a similar way in [33]. The output of a commercial tunable cw Ti:sapphire laser (Spectra Physics 3900S) is attenuated to about 15 mW and then divided by a non-polarizing 50:50 beamsplitter. The signal of one arm is guided to a silicon photodetector (PD2), while the output of the other arm is focused (f = 20 mm) on the gain chip surface with a spot diameter below 25 µm. The gain chip is pumped with the same parameters as presented in Section 4.1. The tunable cw beam is amplified in the gain structure and the reflected signal is detected with an equivalent silicon photodiode (PD1). A chopper is inserted into the laser beam path to determine the offset level of both detector signals. A scheme of the recorded signal is depicted in Fig. 4b. For one data point, 200

#159130 - $15.00 USD Received 2 Dec 2011; revised 19 Jan 2012; accepted 20 Jan 2012; published 3 Feb 2012
(C) 2012 OSA

iterations of the signal analysis are performed. Motorized wavelength tuning together with an optical spectrum analyzer enables feedback wavelength control.

The recorded signal of the VECSEL gain chip $S_{GC}$ is calibrated with the signal from a high-reflective mirror $S_{HR}$ with a known reflectivity $R_{HR}$ [33]. The reflectivity of the gain chip can be described by

$$R_{GC}(\lambda) = R_{HR}(\lambda)\frac{S_{HR,PD2}(\lambda)}{S_{HR,PD1}(\lambda)}\frac{S_{GC,PD1}(\lambda)}{S_{CG,PD2}(\lambda)}, \tag{1.7}$$

where λ describes the probing wavelength.

## 5. Experimental results

### *5.1 Gain saturation measurements*

Using the setup described in the Section 4.1, a systematic study of the gain saturation behavior for different heat-spreading materials, pump intensities, pulse durations and heat-sink temperatures was performed. Figure 5a shows a typical measurement of the VECSEL structure 1 (Table 1).

Recently, we used for our pulse formation simulations a value of $F_{sat} \approx 160$ μJ/cm$^2$ for the gain, a typical value assumed in the literature [17]. As shown in Fig. 5b, we demonstrate that the gain structures actually saturate at much lower fluences in the range between 30 and 80 μJ/cm$^2$. The saturation fluences rise nearly linearly with increasing temperatures both for structure 1 on copper and diamond heat-spreaders, and structure 2 on copper for probing with 1.4-ps pulses. In addition, we measured up to 5.1% small-signal gain (Fig. 5c) with this technique. The unsaturated gain is decreased for increasing temperatures of the heat sink. This will be discussed in Section 5.2. The influence of the temperature on the small-signal gain and the gain saturation is very pronounced. In the ps-regime for structure 1 slightly higher saturation fluences were found than for structure 2. The gain characteristics are dependent on growth influences. Thus it is very difficult to explain small deviations in measurements for both structures, as the spot-to-spot variation for one sample is in the same order of magnitude.

For characterization with 130-fs pulses the saturation fluences were lower than for picosecond pulses. In this regime, carrier heating influences the carrier density and the description of the saturation behavior with a two-level system has to be replaced by a model with modified rate equations [21]. In [34], it was experimentally verified that shorter pulse durations result in decreased intra-cavity fluences because of enhanced gain saturation. This becomes even more significant for pulse durations in the regime of 100 fs and below. These results are in good agreement with our measurements.

#159130 - $15.00 USD Received 2 Dec 2011; revised 19 Jan 2012; accepted 20 Jan 2012; published 3 Feb 2012
(C) 2012 OSA

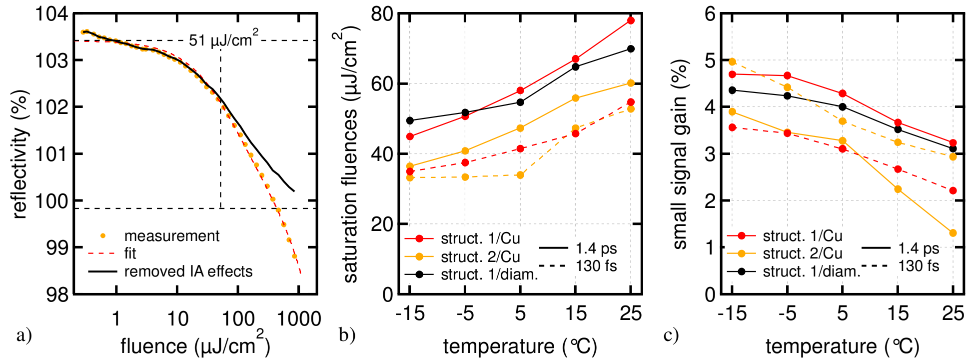


Fig. 5. Saturation fluence measurement data for $\lambda_{centr.}$ ≈960 nm and $I_p$ ≈57 kW/cm$^2$: a) typical gain saturation measurement (QD/diam.): The measurement data (orange) are modeled to the fit function (red) and IA effects are extracted (black); important parameters: $F_{sat}$: 51 μJ/cm$^2$, $F_2$: 60.2 mJ/cm$^2$, $g_{ss}$: 3.58%, $R_{ns}$: 99.85%, $T_{hs}$ = 5°C, $\tau_p$: 1.42 ps, $\lambda_{centr.}$: 959.7 nm. b) saturation fluences in the range of 30-80 μJ/cm$^2$: lower values for 130-fs probe pulses (dashed lines) than for 1.4-ps-pulses (solid line) c) small-signal gain up to 5%: decreased gain with rising heat-sink temperatures.

The improved heat-removal of diamond heat-spreaders can be seen in Fig. 6. As expected the pump intensity dependence in saturation fluence (see Fig. 6a) and small signal gain (see Fig. 6b) is reduced for the diamond heat-spreader.

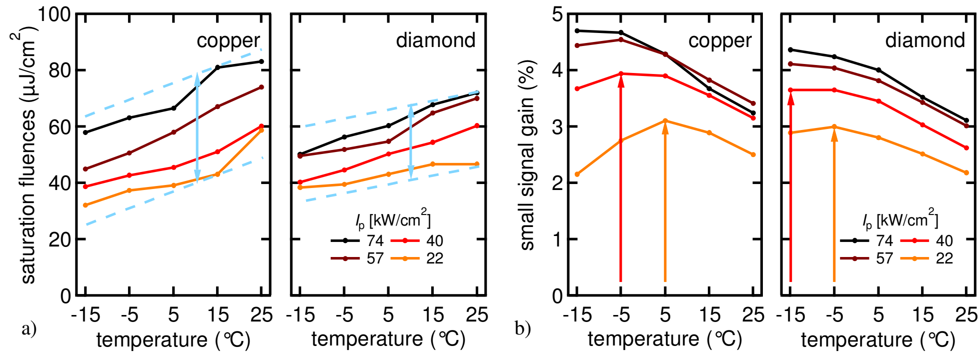


Fig. 6. Influence of heat spreading material on gain parameters of structure 1 (varying heat sink temperatures and pump intensities): a) saturation fluences: *left* copper heat spreader *right:* diamond heat spreader b) *left* copper heat spreader *right:* diamond heat spreader.

At longer pulse duration (i.e. 1.4 ps pulse duration), the effect of IA for the active VECSEL characterization was found to be in the range of $F_2$ ≈ 60-70 mJ/cm$^2$, while analogous measurements of SESAMs (i.e. passive VECSEL characterization without any optical pumping) yields IA of $F_2$ ≈ 35-40 mJ/cm$^2$. At shorter pulse durations of 130 fs the active VECSEL characterization resulted in a $F_2$ ≈ 20-25 mJ/cm$^2$. The combined effects of gain saturation and IA limit the operation of VECSELs to the low-saturated gain regime with lower intra-cavity fluences and therefore lower average output power.

*5.2 Spectral gain characterization*

Similar to the characterization of gain saturation, the influence of the heat-sink temperature and the pump intensity on the small-signal gain is important for optimizing high-power femtosecond operation of modelocked VECSELs. Figure 7 depicts the measured gain spectra

#159130 - $15.00 USD Received 2 Dec 2011; revised 19 Jan 2012; accepted 20 Jan 2012; published 3 Feb 2012
(C) 2012 OSA

for the structures described in Section 2 with pump intensities of 57 kW/cm$^2$ and for the first time, to the best of our knowledge, varying heat-sink temperatures ($T_{hs}$).

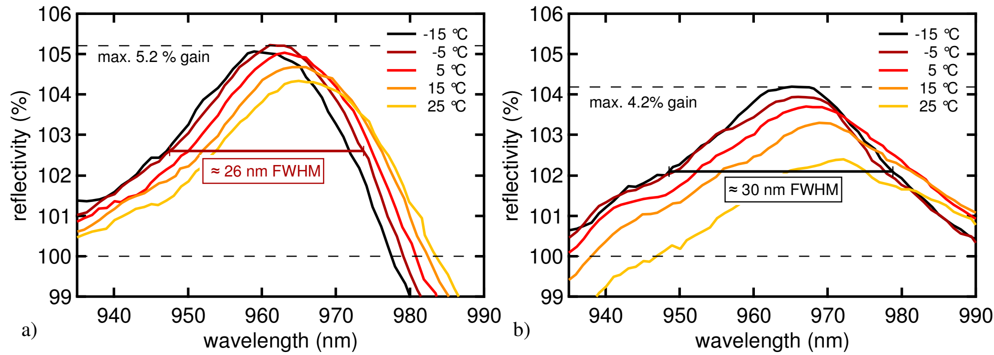


Fig. 7. Gain spectra for different heat sink temperatures at a pump intensity of 57 kW/cm$^2$: a) Structure 1: QD-based structure on diamond heat-spreader with up to 5.2% small-signal gain and b) Structure 2: QW-based structure on copper heat-spreader with up to 4.2% small-signal gain.

A reflectivity exceeding 100% results from unsaturated gain, which determines the small-signal gain. Structure 1on a diamond heat-spreader (see Fig. 7a) exhibits up to 5.2% small-signal gain for $T_{hs}$ = −5 °C. The peak wavelength shifts linearly at a rate of ≈ 0.15 nm/K. Structure 2 on a copper heat-spreader (see Fig. 7b) exhibits up to 4.2% small-signal gain for $T_{hs}$ = −15 °C. The peak wavelength shifts linearly with a rate of ≈ 0.18 nm/K and the small-signal gain drops rapidly with increasing temperature. For multiple layer structures in the active region the theoretically predicted shift-rates of 0.3 nm/K for the bare QWs and 0.1 nm/K for the thermally modified structure can be altered by superimposed effects [3]. In structure 1 the drop of small-signal gain is far less pronounced than for structure 2. This can be explained by the reduced thermal conductivity of the copper heat-spreader. Both structures exhibit broad gain spectra with a maximum FWHM bandwidth of 26 nm (structure 1) and 30 nm (structure 2). For different pump intensities and heat-sink temperatures only a 10% reduction of the maximum bandwidth was identified.

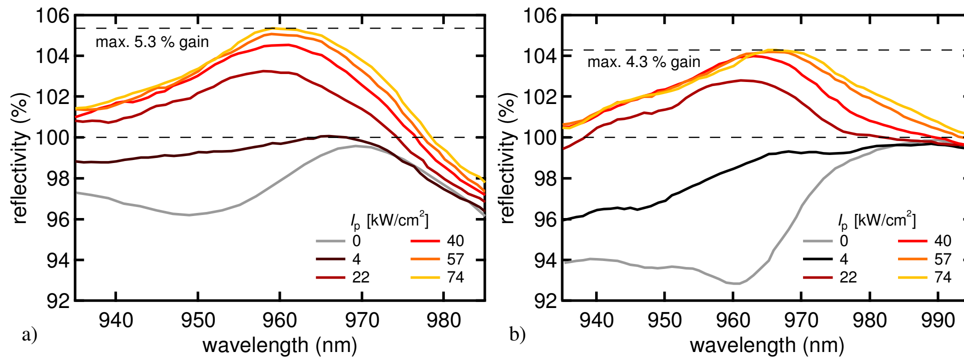


Fig. 8. Gain spectra for different pump intensities at a heat-sink temperature of −15 °C: a) structure 1 on diamond heat-spreader with up to 5.3% small-signal gain and b) structure 2 on copper heat-spreader with up to 4.3% small-signal gain.

With a fixed heat-sink temperature of −15 °C, the build-up of the gain for increasing pump intensities is depicted in Fig. 8. Without pumping, the active regions absorb the light, for increasing pump intensities first transparency is reached and subsequently the gain builds up to a maximum of 5.3% (structure 1, see Fig. 8a) and 4.3% (structure 2, see Fig. 8b). The increased pump intensities result in an enhanced heat deposit in the active region, which

#159130 - $15.00 USD Received 2 Dec 2011; revised 19 Jan 2012; accepted 20 Jan 2012; published 3 Feb 2012
(C) 2012 OSA

leads to a shift of the peak-wavelengths of about 2 nm (structure 1, diamond) and about 5 nm (structure 2, copper) for the same increase of the pump intensity. Simulations of passive modelocking often rely on a parabolic fit of the gain spectrum centered around the lasing wavelength for a simplified description of gain dispersion [35]. The curvature of the parabola $g''(\omega)$ with respect to the optical frequency $\omega = 2\pi c/\lambda$ is calculated for both structures at $T_{hs} = -5$ °C and $I_p = 57$ kW/cm$^2$ (remark: 1% gain equals $g = 0.01$). The parabolic fit for structure 1 results in $d^2g/d\omega^2 = (-95 \pm 15)$ fs$^2$, and for structure 2 in of $d^2g/d\omega^2 = (-75 \pm 12)$ fs$^2$.

Two effects for broadening the gain bandwidth in the structure are discussed. First, the temperature distribution in the structure has to be considered. Surface-pumping with a Gaussian intensity profile together with backside-cooling leads to a temperature gradient perpendicular and along the layer structure. This can shift the emission spectra not only of different succeeding QWs, but also within the spatial profile of the probe laser spot. This results in a broader total gain bandwidth. It is reported that the temperature shift of the gain for bare QDs is a factor of ten less than for QWs [36]. For the presented QD structure (Stranski-Krastranov growth [24] at Innolume GmbH, Germany), the temperature change is in between bare QD- and QW-structures. Secondly, in the QW structure the peak-wavelength for each of the seven wells can vary a few nanometers from its design value because of growth uncertainties, which can broaden the gain bandwidth even more. Calculations yield gain spectra up to 90 nm bandwidth for InAs/GaAs QDs [37], while for multi-QW InGaAs/GaAs structures intrinsic gain up to a bandwidth of 20 nm was measured [38]. Taking the wavelength-dependent field enhancement in the structure into account, the intrinsic gain spectra of the embedded QWs or QD layers have to be much broader than the measured bandwidth. The measurement of the intrinsic gain spectra of the QWs or QD layers is not feasible. However, simple simulations yield that the intrinsic gain spectra of both structures have to exceed 35 nm to result in a gain bandwidth of 26 nm (structure 1) and 30 nm (structure 2) FWHM.

## 6. Conclusion and outlook

We demonstrate for the first time a full gain characterization for VECSEL structures with two high-precision reflectivity measurement techniques.

**Table 2. Experimental Results of the Characterized VECSEL Structures**

| VECSEL gain chip | structure 1 | | structure 2 | |
|---|---|---|---|---|
| | **gain saturation measurements** | | | |
| **saturation fluence** | 1.4 ps: | $F_{sat} \approx 44 - 80$ µJ/cm$^2$ | 1.4 ps: | $F_{sat} \approx 38 - 60$ µJ/cm$^2$ |
| | 130 fs: | $F_{sat} \approx 35 - 54$ µJ/cm$^2$ | 130 fs: | $F_{sat} \approx 32 - 51$ µJ/cm$^2$ |
| **small-signal gain** | 1.4 ps: | $g_{ss,max} \approx 4.7\%$ | 1.4 ps: | $g_{ss,max} \approx 3.9\%$ |
| | 130 fs: | $g_{ss,max} \approx 3.6\%$ | 130 fs: | $g_{ss,max} \approx 5.0\%$ |
| **induced absorption** | 1.4 ps: $F_2 \approx 60$ - 70 mJ/cm$^2$ | | | |
| | 130 fs: $F_2 \approx 20$ - 25 mJ/cm$^2$ | | | |
| | **spectral gain characterization** | | | |
| **small-signal gain** | $g_{ss,max} \approx 5.3\%$ | | $g_{ss,max} \approx 4.3\%$ | |
| **peak gain shift** | for diamond heat-spreader: ≈ 0.15 nm/K | | for copper heat-spreader: ≈ 0.18 nm/K | |
| **gain bandwidth** | ≈ 26 nm (FWHM) | | ≈ 30 nm (FWHM) | |

Table 2 summarizes the experimental results of both measurement techniques using two different VECSELs. We experimentally determined saturation fluences in the range of 30-80 μJ/cm$^2$. Probing with 130-fs pulses reduced the saturation fluence substantially compared to 1.4-ps probe pulses. It was reported in [21] that for shorter pulse lengths gain saturation is enhanced because of increased carrier heating effects that modify the carrier density. In [34], the influence of gain saturation in the sub-200-fs regime was experimentally studied. It was reported, that a shortening of the pulse duration in an operating laser system leads to a decrease in intracavity fluences because of gain saturation. This is in good agreement with the presented measurements. The knowledge of these important VECSEL gain parameters will enable more accurate pulse propagation simulations and will give better insight for the pulse formation process. Taking into account the measured saturation fluence for the gain, further power scaling will require not only different cavity mode adjustments, but also new structure designs with reduced induced absorption.

**Acknowledgments**

The research leading to these results has received partial funding from the European Community's Seventh Framework Programme (FAST-DOT) under Grant No. 224338, and by the Swiss Confederation Program Nano-Tera.ch which was scientifically evaluated by the SNSF.

#159130 - $15.00 USD Received 2 Dec 2011; revised 19 Jan 2012; accepted 20 Jan 2012; published 3 Feb 2012
(C) 2012 OSA